Korean J. Chem. Eng., 39(11), 2907-2915 (2022)
DOI: 10.1007/s11814-022-1272-3

pISSN: 0256-1115
eISSN: 1975-7220

Numerical analysis of the coupling between heat transfer and pyrolysis in heat-not-burn tobacco using computational fluid dynamics

Shin Hyuk Kim*,‡, Hongbum Choi*,‡, Yongmi Jung, and Jay H. Lee*,†**

*Department of Chemical and Biomolecular Engineering, Korea Advanced Institute of Science and Technology, 291 Daehak-ro, Yuseong-gu, Daejeon 34141, Korea
**Korea Tomorrow and Global Corporation, 30 Gajeong-ro, Yuseong-gu, Daejeon 34128, Korea
(*Received 14 March 2022 • Revised 25 July 2022 • Accepted 21 August 2022*)

Abstract−This work developed a computational fluid dynamics (CFD) model to analyze and optimize the design of a heat-not-burn tobacco (HnB) device, which is an electrically heated tobacco product. The associated mathematical models were derived to express the fluid flow and pyrolysis of tobacco porous media, which is assumed to follow Darcy' law. In addition, an apparent kinetic model was implemented as a submodel to represent tobacco pyrolysis reactions. Simulation results of the CFD model were compared with experimental data for validation. The results elucidate the interplay between the heat transfer inside the tobacco substrate and the pyrolysis reactions. Case studies were conducted to reveal that the chemical components generated in the HnB are strongly affected by the temperature distribution inside, which can be controlled by the heater design and operation. This leads us to suggest a new design which has dual heat sources of a needle heater and a wall heater controlled at 468 K. The proposed design is shown to increase the nicotine generation rate by 4.6 times while generating less amounts of harmful and potentially harmful constituents (HPHCs).

Keywords: Electrically Heated Tobacco Product, Heat-not-burn Tobacco, Computational Fluid Dynamics, Heat and Mass Transfer, Pyrolysis

INTRODUCTION

To alleviate the health risks of smoking, new styles of cigarettes are demanded that reduce the inhalation of toxicants. Heat-not-burn tobacco (HnB), a new alternative, is known to generate less harmful and potentially harmful constituents (HPHCs) by thermally decomposing tobacco under a low temperature operation [1]. Unlike the conventional cigarette (c-cigarette), which induces the three reaction stages of evaporation, pyrolysis, and combustion, the new device involves only the first two stages and eliminates combustion by the use of electrical heating. In doing so, it lowers the generation of toxicants such as tar and carbon monoxide [2].

A c-cigarette and an HnB have similar chemical reaction mechanisms. Therefore, past experimental studies on c-cigarettes [3-5] serve a basis for revealing the pyrolysis mechanism in the HnB. Unlike c-cigarettes, which decompose tobacco at high temperature up to 1,200 K, the HnB works with pyrolysis occurring at 400 to 600 K. For this reason, several experimental studies for the development of HnB have analyzed the tobacco smoke generated in a low temperature range [2,6,7], and derived the reaction mechanisms and kinetic parameters [8]. However, these researches have not been able to measure and analyze the phenomena of fluid dynamics, heat transfer, and chemical reactions occurring inside the porous biomass or resin parts of the HnB. The lack of research stands as a hurdle to device development and exploration of mechanical improvements. To this end, additional research is needed to analyze and predict various physicochemical phenomena occurring inside the HnB tobacco segments through numerical modeling and simulation.

In the c-cigarette fields, various research results have analyzed the thermal decomposition of tobacco [9-11]. In addition, CFD simulations combining the transfer phenomena and the chemical reaction kinetics have emerged since the interplay between heat transfer and pyrolysis inside a tobacco stick is critical. Some research works have elucidated the decomposition process of c-cigarettes [12-14] and the effect of the filter which is an auxiliary segment of c-cigarettes [15]. CFD has also been used to analyze the phenomena inside the HnB segments. Works so far have addressed the effect of temperature distribution inside an HnB on tobacco pyrolysis [16] and the development of a CFD model to predict the components of the tobacco smoke generated inside a HnB [17]. However, these studies concentrated on specific designs to compare simulation results with experimental data. To our knowledge, there has been no work on using a CFD model to explore design degrees of freedom for optimal performance.

This work has an ultimate goal of improving the design of HnB with the aid of CFD modeling and simulation. To achieve this objective, we first developed a CFD model of HnB and a numerical procedure to simulate it. The developed model was implemented in ANSYS FLUENT v.19 after combining with a sub-model that calculates the apparent kinetics. The implemented model was par-

†To whom correspondence should be addressed.
E-mail: jayhlee@kaist.ac.kr
‡These authors contributed equally.

tially validated by comparing with experimental data, and then used to obtain insights suggest an improved design. Case studies were conducted to elucidate the interplay between heat transfer and pyrolysis inside tobacco sticks and to arrive at the suggested design, which involves dual heat sources of a needle heater and a wall heater controlled at 468 K.

MODEL DESCRIPTION

This section presents mathematical models for describing the fluid flow, heat transfer, and pyrolysis inside a tobacco stick and briefly explains the numerical solution method employed to solve them together.

1. Governing Equations

The gas phase fluid passing through a HnB stick which is filled with biomass substrates or polymer coolants has a nonlinear flow pattern determined by the porosity and the kinematic coefficient. Darcy's law describes the proportional relationship between the fluid permeability of a substrate and the flow velocity assumed as a laminar flow [17]. Assuming the porous medium and the fluid are in thermal equilibrium, the energy balance equation can be derived based on γ, the porosity of the medium. Thermal decomposition reactions of tobacco medium generate a multi-component gas product which must be described with a compressible flow. The compressibility of the gas can be reflected by the ideal gas equation of state (EOS). The detailed mathematical equations describing the above-mentioned physicochemical phenomena are as follows [19]:

Continuity equation

$$\frac{\partial(\gamma\rho)}{\partial t}+\nabla\cdot(\gamma\rho v)=\gamma S_m \tag{1}$$

Momentum equation

$$\frac{\partial(\gamma\rho v)}{\partial t}+\nabla\cdot(\gamma\rho vv)=-\gamma\nabla P+\nabla\cdot(\gamma\bar{\bar{\tau}})-\frac{\gamma^2\mu v}{\alpha}+\gamma S_m v \tag{2}$$

Energy equation

$$\frac{\partial(\gamma\rho E+(1-\gamma)\rho_s E_s)}{\partial t}+\nabla\cdot(v(\rho E+P)) = \nabla\cdot\left[(\gamma k+(1-\gamma)k_s)\nabla T-\left(\sum_i h_i J_i\right)\right]+S_h \tag{3}$$

Species equation

$$\frac{\partial(\gamma\rho Y_i)}{\partial t}+\nabla\cdot(\gamma\rho v Y_i)=-\nabla\cdot(\gamma J_i)+\gamma S_{m,i} \tag{4}$$

Ideal gas law for the compressible flow

$$\rho=\frac{P_{op}+P}{RT\Sigma_i\frac{Y_i}{MW_i}} \tag{5}$$

where γ is the porosity of the medium, ρ and ρ_s are the density of fluid and solid, v is the velocity, S_m and $S_{m,i}$ are the mass source, P is the system pressure, P_{op} is the operating pressure, $\bar{\bar{\tau}}$ is the stress tensor, μ is the viscosity, α is the permeability of the medium, E and E_s are the total energy of fluid and solid, k and k_s are the thermal conductivity of fluid and solid, T is the system temperature, h_i is the enthalpy, J_i is the diffusion flux, S_h is the heat source, Y_i is the mass fraction, R is the ideal gas constant, MW_i is the molecular weight and the subscript i is the molecular composition of a mixture of acetaldehyde, carbon dioxide, carbon monoxide, nicotine, and water.

2. Apparent Kinetic Model for Thermal Decomposition of Tobacco

As shown in Eq. (6) below, chemical changes that occur in a tobacco medium are described by the Arrhenius formula of apparent kinetics [8].

$$\frac{\partial\xi_{ij}}{\partial t}=A_{ij}e^{-\frac{E_{ij}}{RT}}(1-\xi_{ij})^{n_{ij}} \tag{6}$$

$$S_{m,i}=\sum_j\alpha_{ij}\frac{\partial\xi_{ij}}{\partial t} \tag{7}$$

$$S_m=\sum_i S_{m,i} \tag{8}$$

$$S_h=\sum_i\hat{h}_i S_{m,i} \tag{9}$$

where ξ_{ij} is the conversion rate parameter, A_{ij} is the Arrhenius constant, E_{ij} is the activation energy, n_{ij} is the apparent reaction order, α_{ij} is the total mass emitted, $\hat{h}_i$ is the standard enthalpy of formation, and subscript j is the peak number.

The kinetic parameters used in our simulation study are listed in Table 1. The "peak" listed in Table 1 refers to an active temperature range for a certain reaction and is categorized as peak 1 or peak 2 according to the characteristic of a molecular component. The apparent kinetics can show more peaks depending on the temperature range considered [5]. Since this study considers a temperature range lower than 613 K, peaks above 613 K are not mentioned. Note that the last three components (i.e., carbon monoxide, nicotine, and water) did not show multiple peaks and hence no peak dependence (see Fig. 6).

3. Model Implementation and Numerical Solution

For the CFD simulation, three-dimensional-computational geometry was drawn and meshed as multizone cells. The term multizone here means a combination of hexagonal and tetrahedral finite cells; by using a hex mesh for a simple part and a tetra mesh for a complex part, one can improve numerical stability and accuracy with a uniform mesh size. Through grid sensitivity analysis, we chose to use about 250,000 cells. ANSYS FLUENT v.19 was used to implement the CFD model, and the thermal decomposition of a tobacco was implemented as part of the model by using the user defined function (UDF) feature of the software. The numerical solution process is associated with the pressure-based coupled solver [20]

Table 1. Kinetic parameters for HnB pyrolysis

Component(i)/Peak(j)	E_{ij}	A_{ij}	n_{ij}	α_{ij}
Acetaldehyde peak 1	58.2×10^6	1.13×10^4	1	0.0202
Acetaldehyde peak 2	137.2×10^6	5.56×10^{10}	2	0.0813
Carbon dioxide peak 1	141.2×10^6	4.77×10^{15}	2	0.0078
Carbon dioxide peak 2	99.8×10^6	8.89×10^6	2	0.2316
Carbon monoxide	145.5×10^6	1.96×10^{11}	2	0.0202
Nicotine	91.5×10^6	2.19×10^8	1.5	0.0177
Water	141.3×10^6	7.96×10^{10}	1.5	0.1025

and the spatial discretization is expressed by the second-order upwind method for all variables. Conversion criteria were set at 10^{-3} in terms of absolute residuals for all equations except for the energy equation which was set at 10^{-6}. The time integration of all equations was performed by a first-order implicit method. The apparent kinetic models were integrated using a first-order explicit method (i.e., the forward Euler method) in the UDF.

SYSTEM DESCRIPTION

1. Process Description

As mentioned, an electronic cigarette of the HnB type induces the pyrolysis of a stick containing tobacco by using a low-temperature heat source to simulate conventional smoking. The HnB stick used in the device comprises four segments: substrate, tube, cooling part, and acetate, as shown in Fig. 1(a)). The substrate segment is packed with tobacco and is the region where pyrolysis occurs. The tube segment is used to carry the generated smoke to the user while preventing a potential thermal damage by the heater on the cooling part. The cooling part contains a polymer coolant and generates aerosol drops by cooling the gas. Lastly, the acetate part delivers the produced aerosols to the smoker's mouth.

This study, as shown in Fig. 1(b), (c), simulates only the substrate and tube parts and does not consider the aerosol generation phenomenon, as the research is mainly concerned with the chemical composition of the smoke. However, in the experimental part, the fully composed product is used. Since the temperatures of the cooling and acetate parts are close to ambient, compositional changes affecting the smoke quality are unlikely to occur in them. The simulation domain consists of the outer walls of the tobacco tube and a sharp needle, both of which can serve as heat sources. The central needle is docked into the tobacco substrate, and the outer walls wrap around the tobacco stick.

2. Experiment for Model Validation

An experiment was conducted to check the validity of the model. The experiment evaluates the amount of nicotine emission per puff when an HnB is subjected to multiple puffs. The method of experiment mostly follows the cigar smoking methods from CORESTA (Cooperation Centre for Scientific Research Relative to Tobacco). A rotary smoking machine (model no. RM20H from Borgwaldt) is used to simulate smoking, and the sample tobacco stick is made according to the ISO 3402 method (295 K, humidity of 60%). The extracted gases and particulates are captured by a Cambridge filter pad (glass fiber capture pad). The collected chemical substances are extracted using a stirrer after a pre-treatment solution (2-propanol mixed with n-heptadecane of 150 μL/L and ethanol of 1,000 μL/L) is added. The extracted substances are separated using gas chromatography (Agilent 6890A from Agilent Technologies), and quantitative analysis is performed using the DB-WAX column (30 m×0.32 mm, ID, 0.5 μm film thickness, Agilent Technologies).

3. Scenario for Model Validation

There are various test standards for cigarette evaluation based on product science-based regulation [21]. These standards stipulate a repetitive puffing pattern of an adult smoker. This research complies with the Health Canada Intense smoking regime (CI). According to CI, the single puff shows a puff volume of 55 ml over 2 seconds and its distribution follows the bell-shaped normal distribution curve as derived in Eq. (10). Moreover, the repetitive puffing pattern comprises ten puff steps at 20 seconds intervals, while following the single puff rule.

$$f(x)=\frac{1}{\sigma\sqrt{2\pi}}e^{\frac{(x-\varepsilon)^2}{2\sigma^2}} \tag{10}$$

where σ is the standard deviation, x is the time in a single puff step, and ε is the mean.

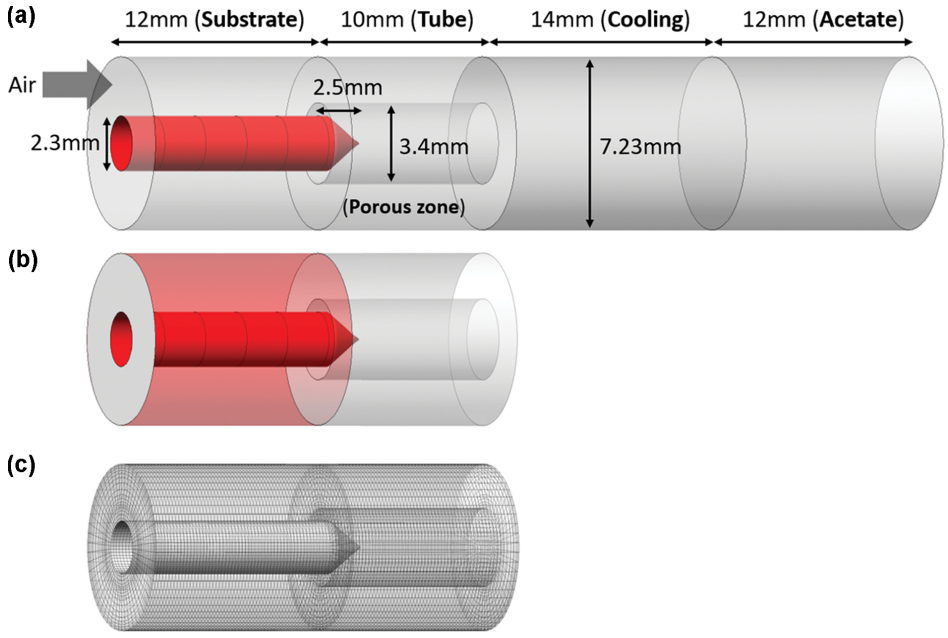

Fig. 1. Design of an HnB stick: (a) schematic diagram, (b) simulation domain, and (c) computational mesh.

Table 2. Operating conditions and physical properties for simulation

	Substrate part	Tube part	
		Inner	Outer
Initial condition	· Pressure: atmosphere · Temperature: 300 K · Component: air		
Boundary condition	· Inlet: pressure inlet (air, 300 K) · Outlet: Mass flow outlet (bell-shape, UDF) · Outer wall: Adiabatic · Heater wall: Temperature (UDF)		
Material	Tobacco	N/A	Polylactic-acid (PLA)
Porosity	0.3		0.6
Absolute permeability (m^2)	4.136×10^{-10}		4.737×10^{-9}
Density (kg m^{-3})	320		1,320
Heat capacity (J kg^{-1} K^{-1})	1,342		1,800
Thermal conductivity (W m^{-1} K^{-1})	0.08		0.13

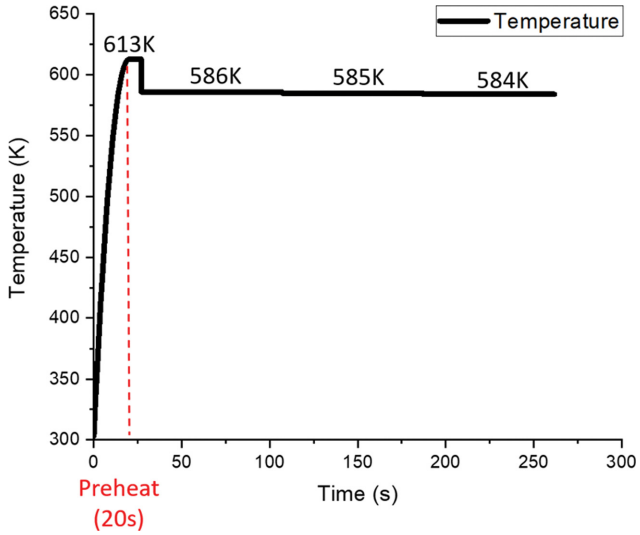

Fig. 2. Temperature profile for the heat source during multi-puffs.

Operating conditions and physical properties for simulation are summarized in Table 2. A database provided in Fluent is used for the physical properties of gas components not shown in the table. Regarding the heat transfer calculation at the wall, with the assumption of laminar flow, the following equation is used which is solved numerically [19].

$$q_w = k\left(\frac{\partial T}{\partial n}\right)_{wall} \quad (11)$$

The HnB requires a heat source to induce tobacco pyrolysis and several options exist. In this study, the in-house control system by KT&G (Korea Tomorrow & Global) corporation was used to control the temperatures of the needle and wall heaters as shown in Fig. 2. The temperature profile represents that for the area-average temperature of the heat sources. In our simulation, the average temperature profile shown in Fig. 2 is entered as a thermal wall condition through the UDF, assuming that a very tight control of the wall can be achieved.

Table 3. Design and operating options for four simulation cases

Case number	Temperature (K)	Heat source	
		Needle-type	Tube-type
1	573	O	X
2	613	O	X
3	573	O	O
4	613	O	O

4. Scenarios for Simulation

This study considered different options for heat sources and temperatures and suggests an optimal one. For simulation scenarios, we initially considered four cases. In the first and second scenarios, a single heater of a needle-type was considered along with two preheat temperatures. The third and four scenarios consider a combination of the needle and wall types (see Fig. 1(b)), again with the two preheat temperatures. The detailed scenarios are listed in Table 3. Operating conditions other than the temperature of the preheater and the heat sources were maintained at the values shown in Table 2. Our analysis of case study results concentrates on the first puff step because the performance of all puff steps levels out when a stable operation is established in the first puff step.

RESULTS AND DISCUSSION

1. CFD Model Validation through Comparison with Experiment

Fig. 3 compares the CFD simulation results against the experimental data to ascertain the accuracy of the implemented CFD model. The amount of generated nicotine for each step over the puffing ten steps was plotted. Notably, large errors are observed on the first and second puff steps since the establishment of thermal stability in the CFD simulation is slowed due to the high permeability of the tobacco tube and the low heat conductivity of the tobacco

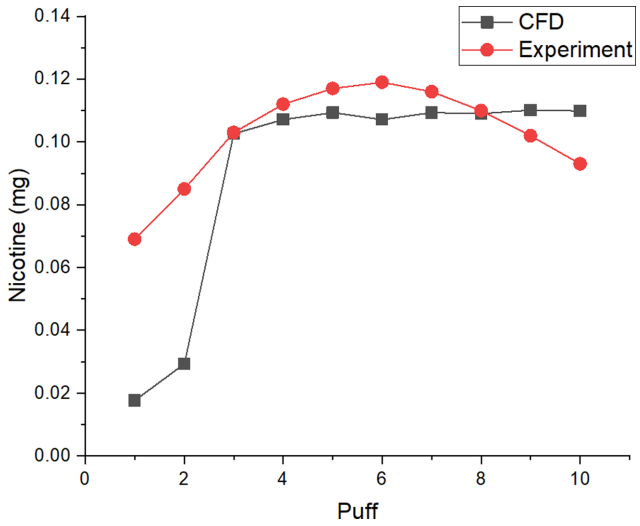

Fig. 3. Comparison of the experimental and simulation data with respect to the mass of nicotine captured per puff step.

substrate. It is difficult to specify the physical properties of the porous media because the sticks are made by filling tobacco with non-regular shape factors with a wide variation range, and therefore, we used our own empirical property values as listed in Table 2. These property values could have been further calibrated to match the data, but this was not done as the focus of this study is on the behavior after thermal stability is established. In addition, the experimental result shows that the amount of nicotine generated decreases after the sixth puff step, whereas the CFD simulation result does not, and this can be attributed to the apparent kinetic model's inability to account for the tobacco quality degradation due to chemical changes by thermal decomposition. Despite the shortcomings, the simulation results are reasonable, showing an average of 11.1% deviations from the experimental data over the ten puff steps.

2. Result Analysis of Multi-puffs Simulation

Fig. 4(a) shows the CFD simulation result of the average substrate temperature over a course of ten puffs. With the temperature profile of the heat source in Fig. 2, the first puff starts at 20 seconds after gradually increasing the temperature by preheating. However, due to the slow heat transfer rate of the tobacco material, the average temperature of the substrate at the first puff is still about 426 K. It rises rapidly to about 470 K at the third puff, after which the temperature rises only slightly. At the last puff, the temperature is 475 K, which is about 49 K higher than at the first puff. The mass fractions of the smoke emitted during ten puffs are calculated by dividing the amount of emission of a component per puff by the total emission amount of the five components per puff, as shown in Fig. 4(b). It can be seen that the emission amount of each component varies until the third puff in accordance with the temperature trend. After that, there are relatively small fluctuations in the mass fractions of the components. At the low temperatures before the third puff, toxicants are mainly produced such as carbon dioxide and acetaldehyde, but as the temperature increases after the third puff, the amount of nicotine increases. This result corresponds to the reaction rates vs temperature curve shown in Fig. 6.

3. Effect of Heat Transfer

Fig. 5 shows for case number 1 the contour profiles of (a) velocity, (b) temperature, and (c) nicotine generation rate. From Fig. 5(a), the flow pattern indicates a laminar flow, and when the air and the generated smoke pass the tube part, the velocity increases toward the direction of the center like in an orifice tube. This flow pattern has been derived by the porous media filled with polymeric protectant against the walls, and the effect of the flow pattern causes the hot fluid to move only through the center, maintaining the wall temperature of the tube part above 300 K as shown in Fig 5(b). In terms of the rate of pyrolysis, as seen from Fig. 5(b) and (c), the generation rate of nicotine is high in the range of 420 K to 480 K, and has a maximum value of about 0.11 kg m^{-3} s^{-1} near 450 K. In addition, the rate of nicotine decreases in the region of high temperature near the needle heater and also in the region of low temperature far from the heat source. These characteristics of tobacco pyrolysis are due to the assumed reaction kinetics, which

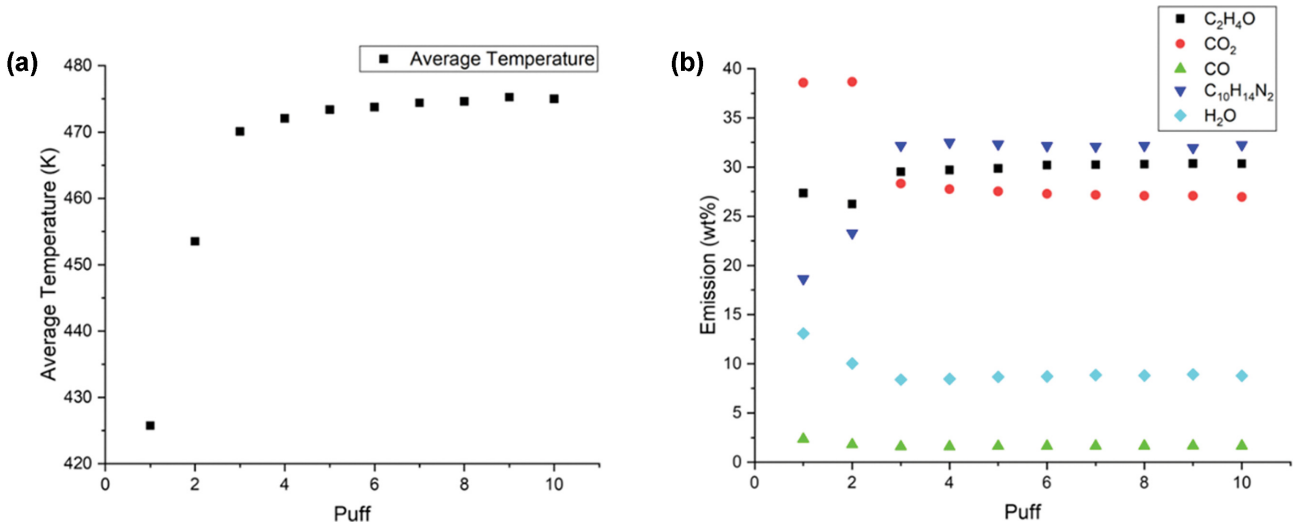

Fig. 4. Analysis of average values over a course of ten puffs: (a) temperature of the tobacco substrate part, and (b) mass fractions (wt%) of the five components in the gas produced.

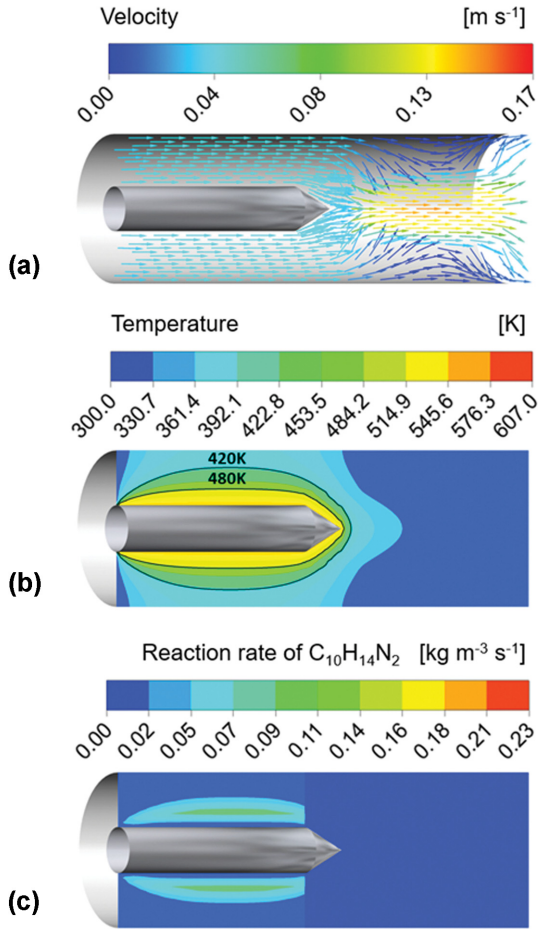

Fig. 5. Vector and contour profiles in a tobacco segment after the first puff: (a) velocity, (b) temperature, (c) emission rate of nicotine.

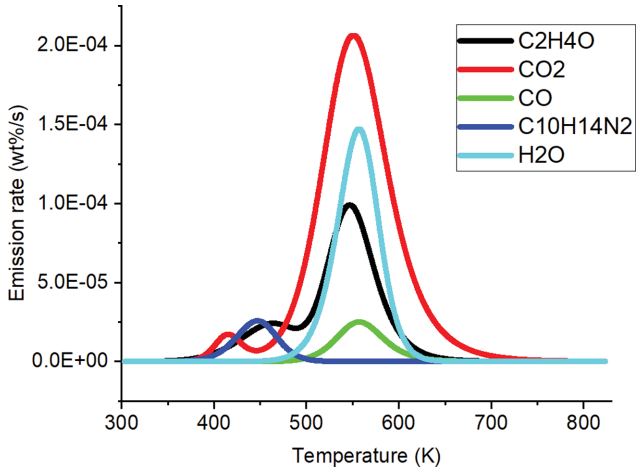

Fig. 6. Reaction rates calculated by the apparent kinetic models.

are highly activated in a specific temperature range. Fig. 6 is the result of simulating the generation rates of acetaldehyde, carbon dioxide, carbon monoxide, nicotine, and water according to the temperature increase based on the apparent kinetics mentioned in

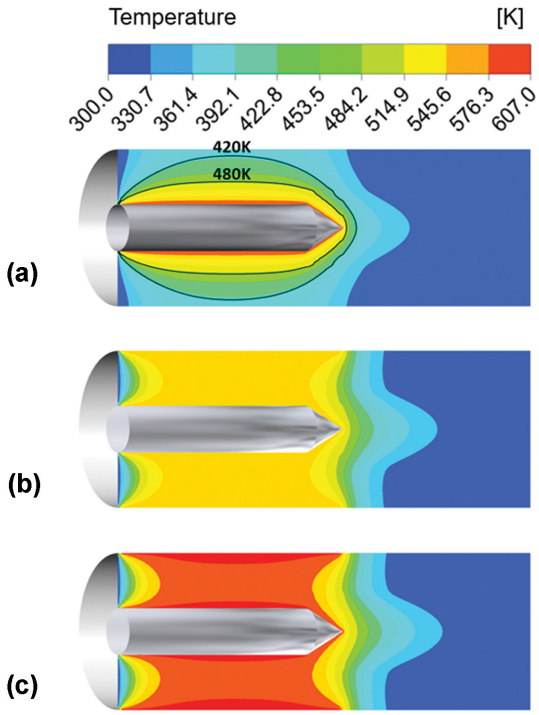

Fig. 7. Temperature contour profiles in a tobacco segment after the first puff: (a) case 2, (b) case 3, and (c) case 4.

Eqs. (6) and (7). The above analysis provides a hint toward an optimal design: The wider the temperature region near 450 K, the higher the nicotine generation.

This section analyzes the effect of increasing the temperature of the heaters or changing the heat source(s) as described by case numbers from 2 to 4. First, Fig. 7(a) increases the preheat temperature to 613 K to accelerate the nicotine generation rate using a needle heater. Fig. 7(b) widens the heat transfer area by about four times by using both the needle heater and the wall heater at 573 K of temperature. Lastly, Fig. 7(c) induces the maximum heating rate by increasing the temperature of the dual heat source to 613 K. In case number 2, the 420 K to 480 K temperature region in the 2D cross section is approximately 1.15 times (1.90×10^{-5} vs. 2.19×10^{-5} m^2) wider than in case number 1, increasing the nicotine generation. In Figs. 7(b) and (c), the use of dual heat sources with a wider heat transfer area leads to more uniform temperature distributions inside the system. However, the heater temperature is set too high in both cases, and temperature in the tobacco tube has risen to an average of 545.9 K and 581.1 K. The raised temperature affects the tobacco pyrolysis pathway to decrease the rate of nicotine generation (see Fig. 6).

Fig. 8 represents the component ratio of the smoke in each case. The nicotine emission in each case is 11.5, 19,9, 3.0, and 0.8 μg which are extracted from CFD results. The highest nicotine occurs when using a single needle heater of 613.15 K as in case 2. However, the concentration of carbon monoxide and water increased together, because the temperature nearby the needle heater was raised and the region of 500 K to 613.15 K promotes the generation of the other components as shown in Fig. 8. Since carbon monoxide is one of the harmful toxicants to smokers, its genera-

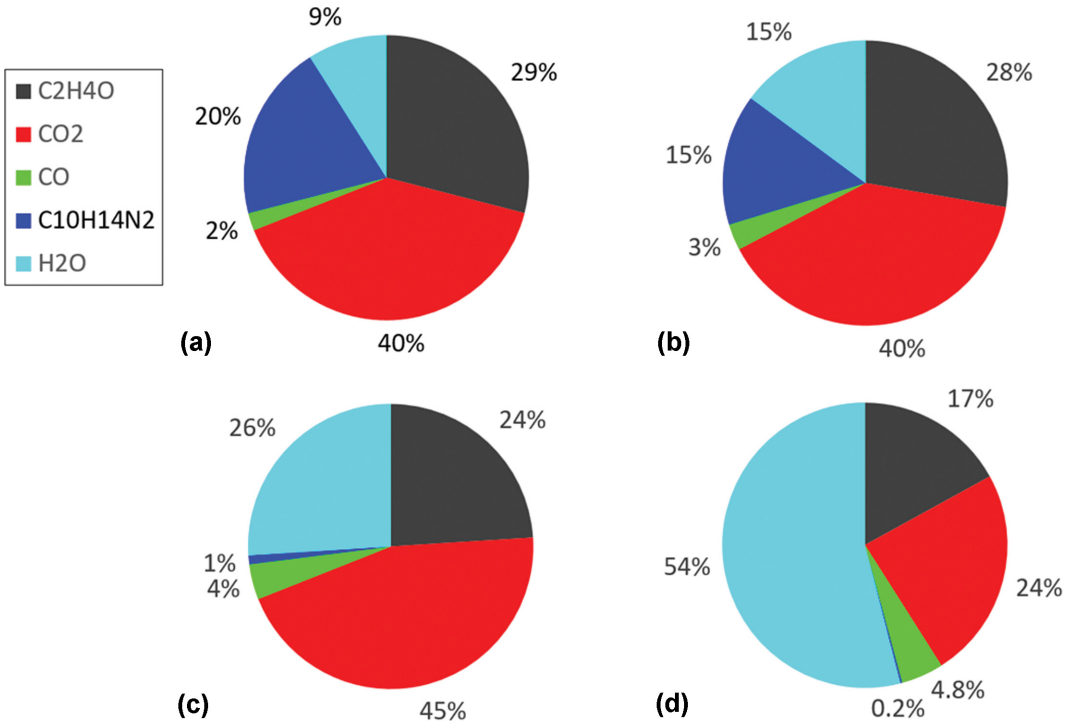

Fig. 8. Component mass fraction of the smoke after first puff: (a) case 1, (b) case 2, (c) case 3, and (d) case 4.

tion should be subdued. Therefore, though case 2 has increased the generation of nicotine compared to case 1, it is questionable whether it represents a superior design. In addition, cases 3 and 4 give low nicotine generation rates of only 1% and 0.2%, because the heat source is too hot and the incoming air during puffing cannot cool the tobacco substrate sufficiently to the optimal temperature range. In addition, the high temperatures in cases 3 and 4 increase the ratio of carbon dioxide and carbon monoxide in the smoke.

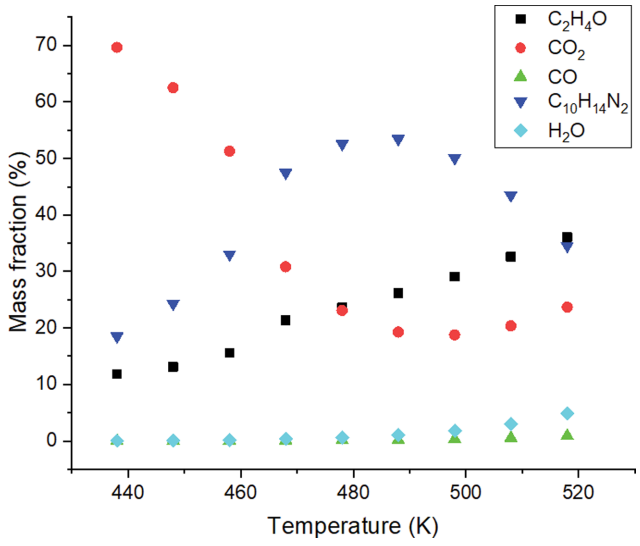

Fig. 9. Component mass fractions of the smoke after the first puff when the suggested two-heater design is used at various heat source temperatures.

4. Suggested Optimization Strategy

The results of sections from 4.1 to 4.3 allow us to set the following objectives/guidelines for designing a HnB device.

1) By maximizing the volume with a temperature of around 450 K, increase the generation rate and ratio of nicotine in the smoke.

2) By minimizing the volume with a temperature over 480 K, decrease the generation rate and ratio of carbon monoxide.

3) By increasing the heat transfer area, reduce the preheating time.

To achieve these three objectives, we proposed the design in Fig. 1(b) and tested the operating temperatures and Fig. 10. The design uses both the needle heater and the wall heater as the heat source. In particular, we tested eight temperature values ranging from 438.15 K (165 °C) to 518.15 K (245 °C) to identify a condition that best satisfies the first and second objectives. As a result, the emis-

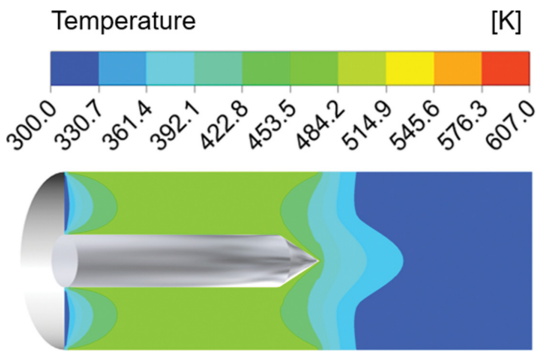

Fig. 10. Temperature contour profile for the proposed design after the first puff.

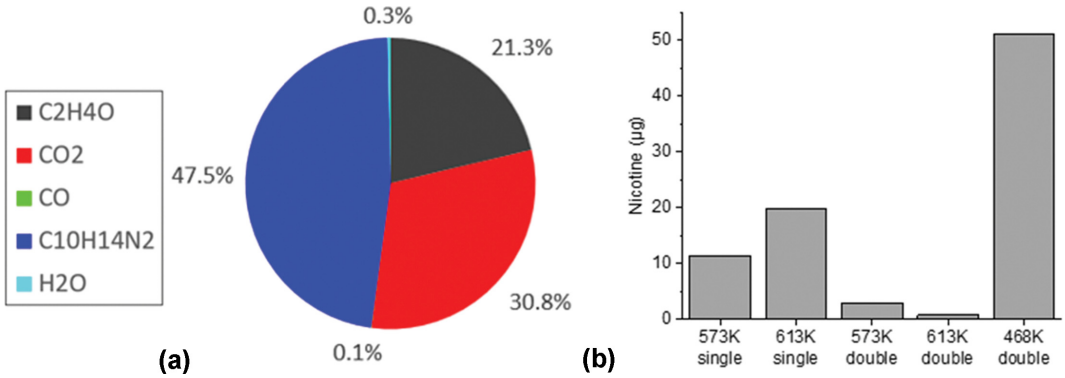

Fig. 11. Characteristics of the smoke for the suggested design after the first puff: (a) Component mass fraction of the smoke, and (b) amount of generated nicotine.

sion of nicotine in the smoke is the highest when the temperature of the heat sources is 488.15 K, as shown in Fig. 9. However, while high nicotine content is more likely to give a good smoke quality, the emission of large amounts of toxicants can harm the user's health. For example, Im, et al. warn that inhaling more than 9 ppm of CO can be harmful to smokers' health [22]. The simulations predict CO emissions of 27.7 ppm at 488.15 K, 13.2 ppm at 478.15 K, and 6.1 ppm at 468.15 K. Based on these results, a heat source of 468.15 K is determined to give the best compromise in the suggested design using the two heaters.

In the proposed design despite maintaining the preheating time of 20 seconds, the temperature inside the tobacco segment reaches the expected value by utilizing a wide heat transfer area. The proposed design stabilizes the temperature within the range of 420 K to 480 K for 90.3% of the tobacco segment volume after the first puff. In particular, the design increases the nicotine ratio in the smoke by about 2.4 times compared to case 1 (compare Fig. 8(a)) and Fig. 11(a)), and also raises the amount of nicotine generated by about 4.6 times in a sing puff step (see Fig. 10(b)). In addition, the proposed design reduces the carbon monoxide emission by 30 times compared to case 2, which had the largest generation rate of nicotine among all the cases.

CONCLUSION

This study developed a CFD model to predict tobacco pyrolysis coupled with heat transfer in an HnB device and explored ways to maximize nicotine generation while minimizing carbon monoxide generation. In particular, apparent kinetic models in the form of ordinary differential equations expressing the thermal decomposition of tobacco substrate were implemented using the UDF feature of ANSYS FLUENT. The associated mathematical models and the numerical solution procedure were explained. The accuracy of the developed CFD model was checked by comparing simulation results with experimental results.

The simulation result has elucidated the interplay between the generation of tobacco smoke and internal heat transfer inside a tobacco stick. It was observed that the yield of nicotine generation improved as the volume of region near 450 K increased. Additionally, the yield of carbon monoxide increased in the region over 480 K. In designing an HnB device, an objective is to maximize the nicotine generation while minimizing the carbon monoxide generation. Based on the simulation results and insights gained, we propose a design that uses both a needle heater and a wall heater as heat sources and controls the heat source temperature at around 468 K. This conceptual design is currently being investigated for possible commercialization by KT&G.

The developed CFD model can be used to further explore ways to reduce the dead zone generated by the injected ambient air. As shown in Fig. 9, even though the heat transfer area of the heater is widened by installing the two heaters, there is a section (e.g., the air entrance part) where thermal decomposition rarely occurs since the temperature is too low. This observation was first made from the CFD simulation, and has given fresh opportunities to improve the design of HnB.

ACKNOWLEDGEMENT

This research was supported by Korea Tomorrow & Global (KT&G) Corporation and Korea Institute for Advancement of Technology (KIAT) grant funded by the Korea Government (MOTIE) (P0008475, The Competency Development Program for Industry Specialist).

NOMENCLATURE

A_{ij} : Arrhenius constant of the component i and the peak number j [s^{-1}]
E : total energy of the fluid [J]
E_{ij} : activation energy of the component i and the peak number j [J $kmol^{-1}$]
E_s : total energy of the solid [J]
h_i : enthalpy of the component i [J kg^{-1}]
$\hat{h}_i$: standard enthalpy of the component I [J kg^{-1}]
J_i : diffusion flux of the component i [kg $m^{-2}s^{-1}$]
k : thermal conductivity of the fluid [W $m^{-1}K^{-1}$]
k_s : thermal conductivity of the solid [W $m^{-1}K^{-1}$]
MW_i : molecular weight of the component i [kg $kmol^{-1}$]
n : local coordinate normal to walls
n_{ij} : apparent reaction order of the component i and the peak

number j
P : system pressure [Pa]
P_{op} : operating pressure [Pa]
R : ideal gas constant [J $kmol^{-1}$ s^{-1}]
S_h : heat source [J $m^{-3}s^{-1}$]
S_m : mass source [kg $m^{-3}s^{-1}$]
$S_{m,i}$: mass source of the component i [kg $m^{-3}s^{-1}$]
T : system temperature [K]
v : velocity [m s^{-1}]
x : time in a single puff step [s]
Y_i : mass fraction of the component i

Greek Letters

γ : porosity of the medium
ρ : density of the fluid [kg m^{-3}]
ρ_s : density of the solid [kg m^{-3}]
$\bar{\bar{\tau}}$: stress tensor [Pa]
μ : viscosity [Pa s]
α : permeability of the medium
ξ_{ij} : conversion rate parameter of the component i and the peak number j
α_{ij} : total mass emitted of the component i and the peak number j
σ : standard deviation
ε : mean (expectation of the distribution)

REFERENCES

1. E. Simonavicius, A. McNeill, L. Shahab and L. S. Brose, *Tobacco Control*, **28**, 582 (2018).
2. M. Forster, C. Liu, M. G. Duke, K. G. McAdam and C. J. Proctor, C. J., *Chem. Cent. J.*, **9**, 1 (2015).
3. R. R. Baker, *Thermochim. Acta*, **28**, 45 (1979).
4. R. R. Baker and L. J. Bishop, *J. Anal. Appl. Pyrol.*, **71**, 223 (2004).
5. M. A. Wojtowicz, R. Bassilakis, W. W. Smith, Y. G. Chen and R. M. Carangelo, *J. Anal. Appl. Pyrol.*, **66**, 235 (2003).
6. M. K. Akalin and S. Karagöz, *BioRes.*, **6**, 1520 (2011).
7. A. Gómez-Siurana, A. Marcilla, M. Beltrán, D. Berenguer, I. Martínez-Castellanos, L. Catalá and S. Menargues, *Thermochim. Acta*, **587**, 24 (2014).
8. F. Barontini, A. Tugnoli, V. Cozzani, J. Tetteh, M. Jarriault and I. Zinovik, *Ind. Eng. Chem. Res.*, **52**, 14984 (2013).
9. M. Muramatsu, *Beiträge zur Tabakforschung International/Contributions to Tobacco Research*, **21**, 286 (2005).
10. S. Talih, Z. Balhas, R. Salman, R. El-Hage, N. Karaoghlanian, A. El-Hellani, M. Baassiri, E. Jaroudi, T. Eissenberg, N. Saliba and A. Shihadeh, *Aerosol. Sci. Technol.*, **51**, 1 (2017).
11. S.-C. Yi, E.-S. Song and M. R. Hajaligol, *J. Fire Sci.*, **19**, 429 (2016).
12. B. Eitzinger and S. Pirker, *Beiträge zur Tabakforschung International/Contributions to Tobacco Research*, **21**, 403 (2005).
13. M. S. Saidi, M. R. Hajaligol and F. Rasouli, *Beiträge zur Tabakforschung International/Contributions to Tobacco Research*, **21**, 157 (2004).
14. M. S. Saidi, M. R. Hajaligol and F. Rasouli, *J. Anal. Appl. Pyrol.*, **72**, 141 (2004).
15. W. Jianhui, D. Wen, Z. Kejun, Z. Xiaobing, P. Bin and L. Huimin, *Tobacco Sci. Technol.*, **48**, 39 (2015).
16. Z. Jiang, X. Ding, T. Fang, H. Huang, W. Zhou and Q. Sun, *J. Phys.: Conference Series*, **1064**, 012011 (2018).
17. M. Nordlund and A. K. Kuczaj, ECI Symposium Series (2016).
18. W. M. Deen, *Introduction to chemical engineering fluid mechanics*, Cambridge University Press, Cambridge (2016).
19. ANSYS, *Fluent udf manual 18.0*, ANSYS, Inc. (2017).
20. ANSYS, *Fluent users guide 18.0*, ANSYS, Inc. (2017).
21. R. Goel, Z. T. Bitzer, S. M. Reilly, J. Foulds, J. Muscat, R. J. Elias and J. P. Richie, *Chem. Res. Toxicol.*, **31**, 325 (2018).
22. B. G. Im, S. W. Kim, J. H. Kang and Y. J. Yang, *J. Korean Acad Fam. Med.*, **22**, 674 (2001).